

# Journal of Materials Chemistry B

Accepted Manuscript



This is an *Accepted Manuscript*, which has been through the Royal Society of Chemistry peer review process and has been accepted for publication.

*Accepted Manuscripts* are published online shortly after acceptance, before technical editing, formatting and proof reading. Using this free service, authors can make their results available to the community, in citable form, before we publish the edited article. We will replace this *Accepted Manuscript* with the edited and formatted *Advance Article* as soon as it is available.

You can find more information about *Accepted Manuscripts* in the [Information for Authors](#).

Please note that technical editing may introduce minor changes to the text and/or graphics, which may alter content. The journal's standard [Terms & Conditions](#) and the [Ethical guidelines](#) still apply. In no event shall the Royal Society of Chemistry be held responsible for any errors or omissions in this *Accepted Manuscript* or any consequences arising from the use of any information it contains.

# New targeting agent in selective drug delivery nanocarriers for treating neuroblastoma.

Cite this: DOI: 10.1039/x0xx00000x

Gonzalo Villaverde,<sup>a</sup> Alejandro Baeza,<sup>a,\*</sup> Gustavo J. Melen,<sup>b</sup> Arantzazu Alfranca,<sup>c</sup> Manuel Ramirez<sup>b</sup> and Maria Vallet-Regí<sup>a,\*</sup>

Received 00th January 2012,  
Accepted 00th January 2012

DOI: 10.1039/x0xx00000x

www.rsc.org/

Novel targeting agents based on *meta*-Iodobenzylguanidine (MIBG) moiety against neuroblastoma were synthesized and biologically evaluated for nanocarrier vectorization. These compounds have been anchored on the surface of drug loaded mesoporous silica nanocarriers causing improved cellular uptake in tumoral cells. Neuroblastoma (NB) is the most frequent extracranial pediatric tumor. Advanced forms of the disease (metastatic and/or refractory) have a dismal prognosis despite the combination of chemotherapy, radiotherapy, surgery and bone marrow transplant. These treatments carry severe side effects and, in some cases, compromise the patient life. MIBG has been widely applied in medical diagnosis of NB due to its affinity for the tumor cells through the norepinephrine transporter (NET), which is expressed in 90 % of NB. The exclusive accumulation of MIBG in neuroblastoma has been widely studied; however, its properties have been never exploited as targeting agent in nanocarrier drug delivery systems. Several structural analogues of MIBG have been prepared and attached on the nanocarrier surface. Their selective internalization has been tested against human neuroblastoma cells showing, in the best case, four times higher cellular uptake versus the naked nanosystem. Furthermore, *in vivo* experiments showed preferential and selective accumulation and retention of targeted nanosystem comparing with the naked and the just PEGylated counterpart systems. This novel nanosystem could be easily applicable for all kind of drug delivery nanocarriers, allowing a universal tool for neuroblastoma chemotherapies in the way to step down the classical approaches providing a newfangled nanosystem exclusively designed against this terrible malignancy.

## Introduction

In recent years, the use of nanocarriers as selective drug transporters and theranostic proposes has attracted much attention in nanomedicine applied to oncology. One of the biggest extra-benefits of using drug nanocarriers against cancer is that they can overcome some of the major limitations of conventional chemotherapy such as solubility issues associated with the frequently hydrophobic nature of cytotoxic drugs, short circulation lifetime and typical lack of selectivity.<sup>1</sup> These problems are already addressed through the use of high doses in the treatment. This fact promotes the damage in healthy tissues causing the typical side effects associated to conventional chemotherapy.

In order to improve the selectivity of the nanomedicines specific targeting agents have been designed along the years.<sup>2</sup> These targeted nanosystems are able to transport the cytotoxic compounds specifically to the target cells, and to release their payload once there. This fact causes the destruction of the malignant cells while minimizing the collateral damages in the surrounding tissue.<sup>3</sup> For this reason, the development of new

selective active targeting agents have become into one of the main challenges in nanomedicine.

During last years, efficient ligand-receptor active targeting motifs such as RGD<sup>4,5,6</sup> and folate,<sup>7,8,9,10</sup> are commonly grafted on many different kinds of nanosystems surface for vectorization proposes. Furthermore, new specific moieties with multiple functionality using several types of cell-penetrating peptides,<sup>11,12,13</sup> or vasculature targeting antibodies,<sup>14,15,16</sup> have been recently reported.

The tumoral tissue accumulation characteristics of the nanoparticles is mainly possible due a specific passive targeting effect, which is based on the characteristic tumoral blood vessel architecture. These vessels present large pores and fenestrations of diameters up to few hundred nanometers. When the circulating nanoparticles reach a tumoral site, they pass through these pores being accumulated during longer times within the zone.<sup>17</sup> Further, tumoral tissue also exhibits a poor lymphatic drainage. Both characteristics constitute the well-known enhanced permeation and retention effect (EPR) and is one of the main advantages constituting the basic of the goal standard of the use of nanoparticles in oncology.<sup>18</sup> However, not all the cells which form a tumoral mass are malignant due the great

heterogeneity of these tissues that contain a large number of healthy supportive cells.<sup>19</sup> The functionalization of the nanoparticle surface with molecules (targeting groups) able to be specifically recognized by the tumoral cells constitutes the so called active targeting. The presence of these groups is essential for enhancing the therapeutic efficacy of the nanomedicines.

In this work, we are interested in developing effective nanocarriers that can be applied for neuroblastoma (NB) therapy. NB has being onto one of the challenging problems in pediatric oncology. This disease is the most frequent extracranial pediatric tumor which presents a dismal prognosis despite the combination of chemotherapy, radiotherapy, surgery and bone marrow transplant.<sup>20</sup> Thus, the development of nanocarriers able to detect and destroy only the diseased cells may constitute a significant improvement in the treatment efficacy.<sup>21</sup>

As mentioned above there is a wide range of studies which analyze the vectorization effect of generalist cancer targeting agents in nanoparticles. Bulky targeting agents such as, proteins, large peptides, aptamers, antibodies, *etc.*, are commonly used. However, these agents have several possible binding interaction points, and are usually suitable to interact with unspecific proteins. Otherwise, small molecules with less binding spots may go unnoticed in this media. This fact could make the specific small moieties tolerable to body fluids maintaining its recognizing abilities only with the desired target. In special cases, some types of diseased cells have intrinsic and particular receptors that make it possible to improve the differentiation to each other. Thus, following this philosophy and looking for selective internalization in NB cells, *meta*-Iodobenzylguanidine (MIBG) looks the most suitable candidate for tuning the nanocarrier surface with vectorization proposes.<sup>22</sup> MIBG targeting properties have been applied in conventional medical diagnosis of NB in the last decades due to its affinity by the norepinephrine transporter (NET) which is expressed in 90 % of NB tumors.<sup>23</sup> Because its high specificity for NB and other neuroendocrine tumors; MIBG effectiveness as tumor-targeted vehicle has been also applied in the therapeutic treatment by directed radiation using radioactive iodine (<sup>131</sup>I).<sup>24</sup> Additionally, non-radioactive derivate has shown anticancer activity by itself.<sup>25</sup> The conjugation of MIBG with antitumoral drugs not only enhances their selectivity against tumoral cells but also improves their cytotoxic capacity through synergic effect caused by tumor selective acidification by enhancement of glycolytic flux.<sup>26</sup> This synergy may convert non-radioactive MIBG analogues into important targeting agent within the nanomedicine arena.

MIBG-NET interaction may able to bring the nanosystem to NB cell internalization excluding healthy cells from the process. NET binding pocket is naturally designed for the recognition of small molecules which means that the size of the targeting motifs is limited. The binding mechanism is based on

three main interactions: van der Waals interactions produced by several hydrophobic moieties from NET protein with the aromatic ring of the norepinephrine structure; several weak polar interactions through hydrogen bonds, and, the key one; the ionic interaction between carboxylate group from Asp75 from NET pocket and the protonated amine group from norepinephrine.<sup>27</sup> Not by chance, MIBG is structurally close to norepinephrine, containing an aromatic core backbone responsible for the hydrophobic interactions and benzyl guanidine unit ( $pK_a = 12$ ) able for proton capture which form a similar cationic specie than the norepinephrine amine group. (Figure 1).

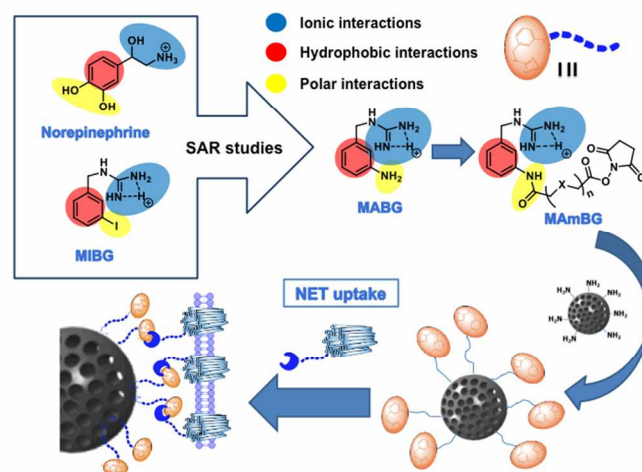
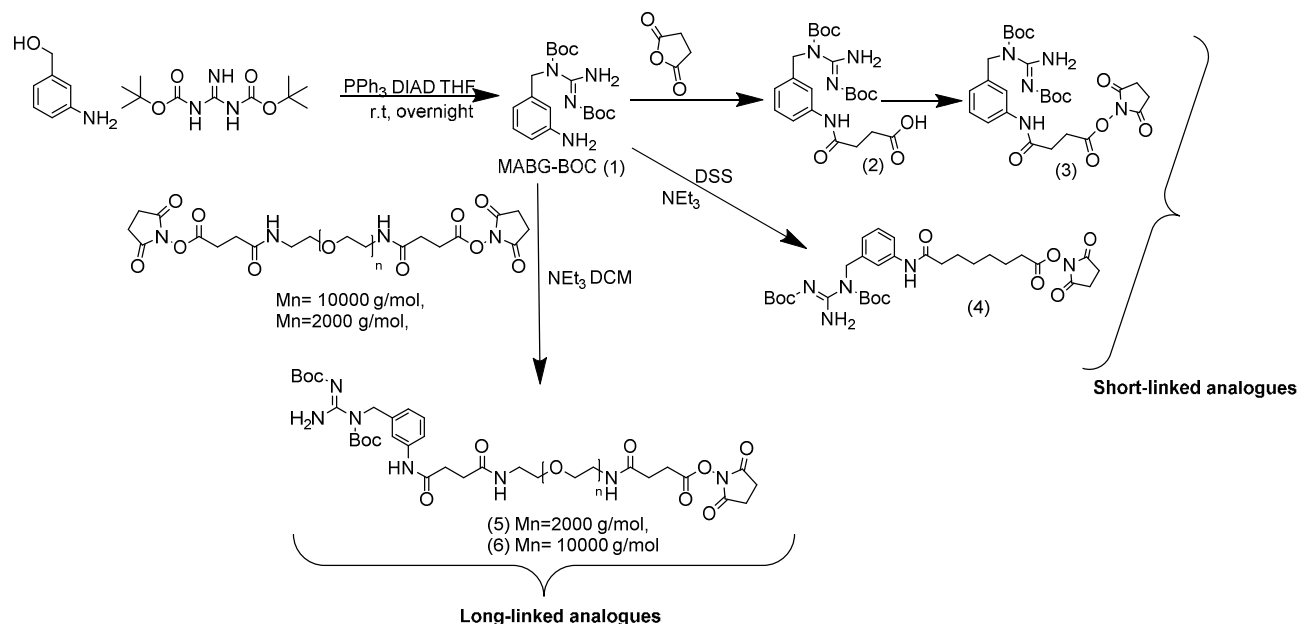


Figure 1. Structural equivalence between Norepinephrine, MIBG, MABG and MAmBG analogues. attachment on MSN and NET uptake.

The possibility to perform structural modifications of MIBG in order to study and improve its uptake selectivity for norepinephrine transporter (NET), has been widely discussed.<sup>28,29,30</sup> Several groups have been incorporated all sorts of variations in *para*- position of the aromatic ring and even the aromatic ring have been replaced by a naphthyl or dibenzoazepine moiety without a significant loss of selectivity for the NET receptor.<sup>31</sup> However, some authors suggest that the substitution of hydrogen in position 5 of the benzene ring is unfavourable for binding NET.<sup>32</sup> On the other hand, the absence of the iodine atom in *meta*-position does not affect the uptake/selectivity properties.

These previous structure-activity relationship studies (SAR) guided us to design, as a first approach, the synthesis of *meta*-aminobenzyl guanidine (MABG) as MIBG analogue. MABG represents one of the simplest structurally accessible approximations to MIBG which keep the same aromatic ring and the guanidine recognition moiety in the same position. On the other hand, substitution of the iodine atom with amino group provides the grafting point to the nanoparticle surface through amide formation (Figure 1).



**Scheme 1.** Synthesis of MAmBG analogues.

PPh<sub>3</sub>: Triphenylphosphine, DIAD: Diisopropyl azodicarboxylate, THF: Tetrahydrofuran DSS: Suberic acid bis(N-hydroxysuccinimide ester), Tol:Toluene, DCM: Dichloromethane, DIC: N,N'-methanedilydenebis(propan-2-amine), NHS: N-hydroxysuccinimide, NEt<sub>3</sub>: Triethylamine.

The new analogue maintains the intrinsic properties from the original MIBG and makes the structure easy functionalizable for the further grafting step on MSN surface.

Furthermore, the use of this amine/amide *meta*-substitution has been reported in tumor detection by Wang *et al.*<sup>33</sup> with promising results in terms of selective accumulation in diseased tissues. However, this type of targeting agents have been never applied on nanocarriers for drug delivery.

## Results and discussion

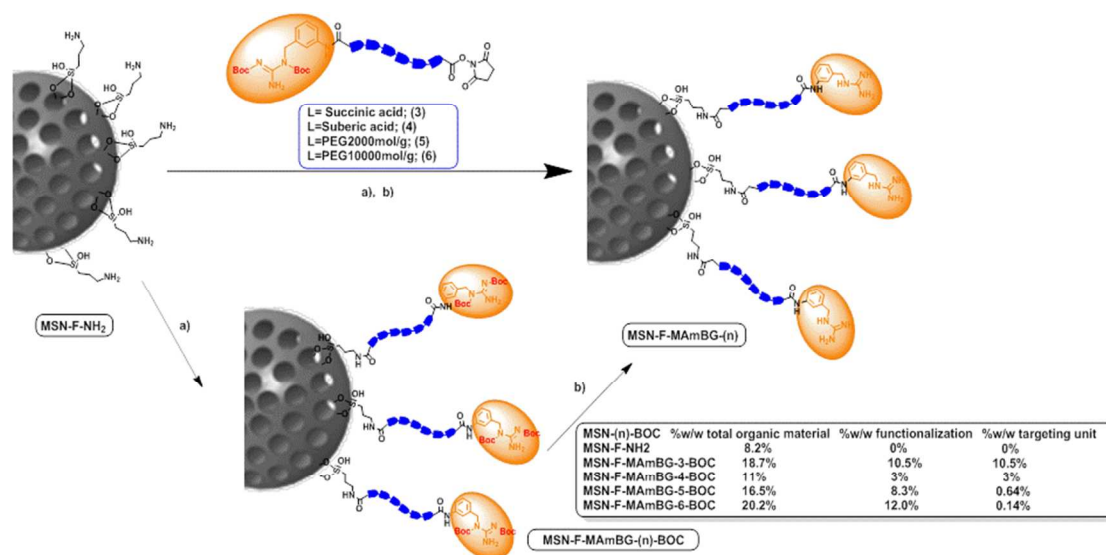
Herein, we report for the first time the use of novel MIBG analogues attached to mesoporous silica nanoparticles (MSN) used as nanocarrier model. These nanosystems are able to exclusively drive cytotoxic drugs to NB cells with minor impact for healthy supportive cells which are usually present in tumor mass. MSN have been widely used for nanomedicine proposes due to their excellent properties as easy functionalization, synthetic versatility, high loading drug capacity and economically low cost starting materials, among others.<sup>34,35,36,37</sup> Furthermore, the external surface of these carriers can be easy decorated with targeting motifs which improve the selectivity and enhance the uptake rate in the malignant cells through receptor–ligand interactions.

The attachment of MIBG based targeting compounds on MSN loaded with cytotoxic drugs could improve both the cytotoxic

response and selectivity of the administered nanomedicines against NB cells.<sup>38,39,40</sup>

In order to facilitate the monitorization of the cellular uptake process, MSNs were synthesized carrying fluorescein moieties covalently attached within the silica matrix following a variation of Stöber<sup>41</sup> and van Blaaderen<sup>42</sup> method. At the same time, amino groups were introduced on the external surface of the nanoparticles through this delayed co-condensation procedure yielding the naked material MSN-F-NH<sub>2</sub>.

The XRD patterns for MSN-F-NH<sub>2</sub> (See S.I., section B.1) shows three of the four low-angle reflections in the 2θ range 2–8° typical of a hexagonal array as (100), (110), (200). These measurements suggest that the pore order was not affected by the introduction of fluorescein and the amino functionalization. A reduction of the peak intensity observed in (210) was not interpreted as a crystallinity lost but rather to a reduction in the X-ray scattering contrast in high functionalized material. Nitrogen absorption measurements showed a value for the total specific surface of 1192 m<sup>2</sup>/g and the adsorption/desorption isotherm is typical of non-filled mesoporous structure with a pore diameter of 2.5 nm. The size distribution profile of the nanoparticles was determined by dynamic light scattering (DLS) showing an average diameter of 190 nm which was confirmed by scanning electronic microscopy (SEM).



Scheme 2. Targeting attachment on MSN. a) THF, corresponding analogue, 40°C, overnight b) DCM, TFA, reflux, 72h.

The presence of amino groups was confirmed by thermogravimetric analysis (around 8% in weight of organic material), FTIR and cross-polarization magic-angle spinning  $^{13}\text{C}$  CP MAS solid state NMR. These amino groups will be employed as anchoring point of the targeting agents through amide formation reactions. Additionally, the free amino groups provided a positive charge (+40 mV) on the particle surface measured by zeta potential which enhanced the colloidal stability of these particles.

MAmBG-type targeting agents were synthesized from a common starting material MABG-BOC (1), which was obtained from 3-aminobenzylalcohol and *N,N*-bis(*tert*-butyloxycarbonyl) guanidine. The reaction follows a variation of a Mitsunobu process previously reported for guanidination of benzyl alcohols and affords the desired analogue with good yields.<sup>43,28</sup> Then, MABG-BOC (1) was functionalized through amide group formation with the desired linkers which contain an activated acid group at the end of their chain yielding the MAmBG derivatives (Scheme 1).

This methodology provides a versatile pathway to explore the influence of the linker chain length in the cellular internalization. Two different categories of MAmBG analogues have been produced. One based on the use of short linkers between the grafting point and the targeting moiety (compounds 3 and 4, Scheme 1). And second, based on the use of longer linkers composed by polyethyleneglycol (PEG) chains of 2 and 10KDa of molecular weight, respectively (compounds 5 and 6, Scheme 1). Besides to separate the targeting agent far away from the surface which improves its interaction with the NET receptor, PEG linker may enhance the circulation time of the nanocarrier inside the blood stream through opsonisation abolition.<sup>44</sup> This effect can be explained due steric interference from PEG chains that make the opsonins not able to be attached on the particle surface. Opsonization is the first step which allows that the nanoparticles will be

recognized by the immune system leading to their clearance. System PEGylation increases the circulation time of nanoparticles that is essential for improving EPR effect efficacy. However, using longer PEG chains could affect the selectivity by shielding the targeting moiety reducing the possibilities of active uptake process.<sup>45</sup>

The first MAmBG analogue, compound (3), was synthesized through two consecutive steps by treatment of MABG-BOC (1) with succinic anhydride affording isolated compound (2) in quantitative yield, following by transformation of the resulted acid in the corresponding activated succinimide ester (3). Compound (4) was obtained by direct reaction of MABG-BOC (1) with DSS in presence of  $\text{NET}_3$ . Long linked analogues were synthesized following the same methodology using commercially available PEG derivatives with double activated acid groups in both ends of the chain (for more synthetic information see S.I section A.1). The amounts of the MAmBG motif in each long linked compound were determined by UV spectrometry (See SI section A.2). The amount of benzylguanidine found in MAmBG-PEG2000-NHS (5) and MAmBG-PEG10000-NHS (6) was 7.7% w/w and 1.2% w/w, respectively. These data indicate that the reactions were resulted in around 50 % of yield in both cases, which was corroborated by  $^1\text{H-NMR}$ . The presence of the second activated acid group in the other side of the chain after condensation process was checked to ensure the posterior grafting process. (See S.I. section A.1).

Deprotection of the BOC groups in all the synthesized analogues, makes the resulting compounds poorly soluble in most of solvents, except methanol or water. This fact, convert their isolation in a tedious process. Additionally, it was necessary to employ forced conditions refluxing the media during 72h to obtain acceptable deprotection yields. Even then, unprotected MABG was isolated, however succinic derivate compound (2) lead its undesired meta-pyrrolidine derivate after

deprotection treatment through acid catalyzed cyclization. (See S.I, section A.1, MPyBG). Therefore, we decided to anchor the BOC protected MAmBG analogues on the silica nanoparticles and once there, to carry out the BOC deprotection in order to make easier the BOC residues elimination and abolishing possible secondary products.

Functionalization of nanoparticles always means a new challenge; one of the parameters more sticky in the synthesis of new hybrid material is to control the amount of organic material covalently immobilized on the surface. Parameters as steric hindrance and charges, in both, nanoparticles surface and organic material, are key parameters for optimal immobilization. For this reason, optimization of the ratio of the MAmBG analogues in front of amine groups available for reaction in the surface is a must in each case. Acid activated MAmBG analogues were covalently grafted on MSN-F-NH<sub>2</sub> by addition of the corresponding compound to a dispersion of nanoparticles in THF at 40°C for 24 h, affording the materials MSN-(n)-BOC. Posterior BOC deprotection treatment with TFA/DCM yields the materials MSN-F-MAmBG with the MAmBG targeting moiety available to bind with NET (Scheme 2). The amount of organic material covalently attached on the MSN surface was determined by TGA resulting in approximately 18.7 % (MSN-F-MAmBG-3-BOC), 11 % (MSN-F-MAmBG-4-BOC), 16.5 % (MSN-F-MAmBG-5-BOC) and 20 % (MSN-F-MAmBG-6-BOC). The amount of targeting agents incorporated in each case was determined assuming a 1:1 equivalence in the case of the short linked analogues (3) and (4) and 7.7% w/w and 1.2% w/w for (5) and (6) respectively (previously calculated by UV spectrometry determination). In all cases, it should be considered that the blank material (MSN-F-NH<sub>2</sub>) has 8.2% w/w of organic material. Thus, the estimation of the targeting moiety functionalization in deprotected materials was 10.5 % and 3 % w/w for MSN-F-MAmBG-3 and MSN-F-MAmBG-4 respectively, and 0.64 % and 0.14 % w/w for MSN-F-MAmBG-5 and MSN-F-MAmBG-6 as maximum values. Obviously, the amount of MAmBG in PEGylated materials were lower than in the short linked. This fact may be attributed to both; the reaction conditions and the steric hindrance of the PEG chains. However, less amount of targeting motif does not mean a minor selectivity, because the targeting agent may be more exposed in this case being more accessible for the interaction with the NET pocket.

The presence of functional groups characteristic of MAmBG derivatives grafted on the nanoparticle surface was confirmed by cross-polarization magic-angle spinning <sup>13</sup>C-NMR solid state. The spectra for each group of the shorter linked analogues were confronted with their counterparts in liquid state before immobilization, for both protected and unprotected materials as Figure 2 shows for MSN-F-MAmBG-3. <sup>13</sup>C CP MAS solid state NMR spectra of short linked material MSN-F-MAmBG-3, both BOC protected and deprotected are totally recognizable in view of the corresponding derivatives before functionalization.

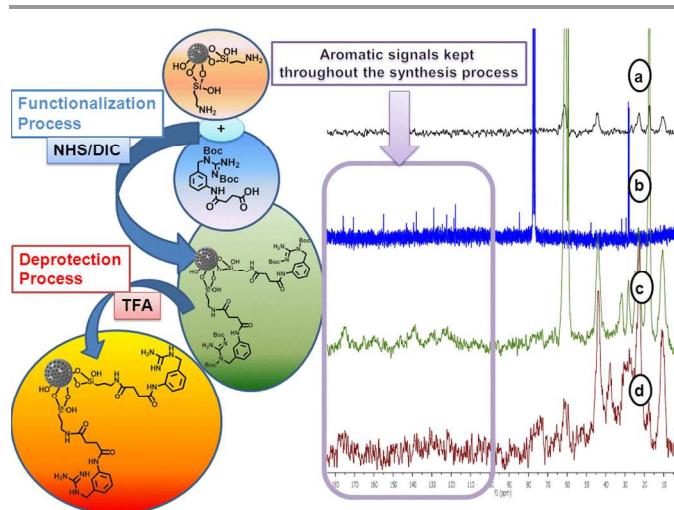


Figure 2. Following the synthesis of MSN-F-MAmBG-3 by <sup>13</sup>C CP MAS-NMR solid state spectra. a) MSN-F-NH<sub>2</sub> b) MAmBG (2) in chloroform c) MSN-F-MAmBG-3-BOC d) MSN-F-MAmBG-3.

The successful grafting process was confirmed by the apparition of the typical signals of MAmBG at approximately 175 ppm (C=O) and 165 ppm (C=N), and undefined broad signals in down field corresponding with aromatic ring from benzylguanidine (Figure 2).

On the other hand, the spectra in the case of long linked analogues MSN-F-MAmBG-5-BOC and MSN-F-MAmBG-6-BOC shows a dominant signal at 72 ppm (CH<sub>2</sub>) from PEG moiety which hide the rest of signals except the classical APTES signals which appears in all of them (See S.I, section B2 for more spectral data). Indeed, the PEG signal clearly indicates the presence of the PEG chains and, as consequence, the success of the functionalization process. Unfortunately, the *tert*-butyl signals from BOC protective group overlap with the APTES moiety and others aliphatic signals (CH<sub>2</sub> from linker moieties) appearing as broad peaks. This fact makes impossible to determine the deprotection grade of the guanidine groups after the treatment with TFA by NMR. However, zeta potential measurements showed changes in the surface charge before and after the deprotection step, as show Table 1.

In general, the surface charge becomes more positive after BOC deprotection which is in agreement with the presence of free guanidine groups. Finally, the organic material determination by TGA reveals, in all cases, that the amount of organic material after functionalization is higher and it suffers a slight decrease after BOC deprotection. According with the DLS measurements, the functionalization process barely alters the nanoparticle size which is a very important aspect in drug delivery for antitumoral therapy (Table 1 and Figure 3a). The preservation of the particle size and the mesoporous structure of each material were confirmed by high resolution SEM and TEM (Figure 3b and 3c)

Table 1. Characterization of MSN-F-MAmBG-n nanomaterials.

Non-Pegylated materials		MSN-F-NH <sub>2</sub>	MSN-F-MAmBG-3-BOC	MSN-F-MAmBG-3	MSN-F-MAmBG-4-BOC	MSN-F-MAmBG-4
	Z.Pot (mV)	+40	+36.6	+29.0	+24.1	+35.6
	Size (nm)	190	176.5	190	214	231
Pegylated materials		MSN-F-MAmBG-5-BOC	MSN-F-MAmBG-5	MSN-F-MAmBG-6-BOC	MSN-F-MAmBG-6	
	Z.Pot (mV)	+19	+24.2	+12	+35.3	
	Size (nm)	208	237	214	226	
O.M % (w/w)	16.4	12.5	20.22	15.5		

O.M :Organic Material.

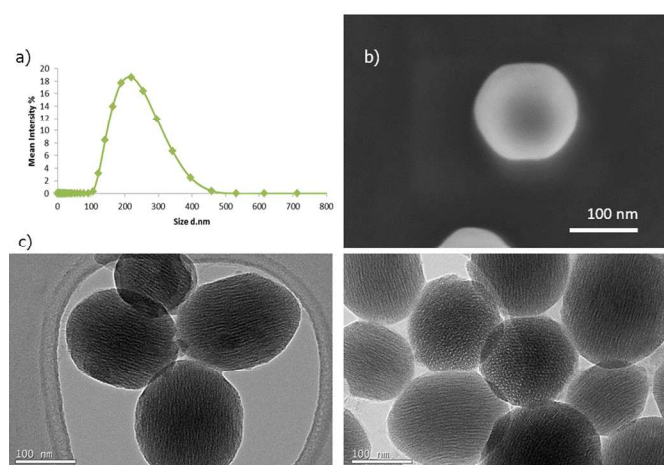


Figure 3. a) Size determination by DLS measurement. b) SEM micrographs of MSN-F-MAmBG-3 scale bars correspond to 100 nm. c) TEM micrographs of MSN-F-MAmBG-5 scale bars correspond to 100 nm.

Finally, XRD show that pore order was maintained after both functionalization and BOC deprotection processes in all materials. (See S.I sections B.2 and B.3). As mentioned above, there is a wide range of studies which analyze the vectorization effect of cancer targeting agents in nanoparticles. The nanosystems studied by *in vitro* assays, show selective avidity and internalization behaviour for tumor cells excluding the healthy ones. However, this effect is attenuated in replications of biological environment as multiprotic serum through the formation of protein corona in the nanoparticle surface.<sup>46,47</sup> The interaction between the surface of the nanosystem and human body fluids is wholly influential in the targeting abilities of the nanosystems. The formation of protein corona in their surface changes the original physical-chemical properties of the entire system. This fact must be taken into account in order to perform a strict evaluation of the targeting effect of the grafted derivatives.

Usually, there are two differenced protein layers; the hard corona, formed by small size proteins, which is the closer and binder with the nanoparticle surface, and, the soft corona, formed by higher size proteins weakly bounded.<sup>48,49</sup> The formation of the protein shell not only could diminish the internalization properties of the nanoparticles but also may hinder the targeting agent properties by protein unspecific interactions with undesired receptors. Thus, both; previous characterization of the nanosystem in serum multiproteic media and internalization assays in tumor environment emulsion are essential. For this aim, the four targeted nanovehicles, as well as non-targeted nanomaterial MSN-F-NH<sub>2</sub> were incubated in multiproteic serum Hyclone (36 g/L of estimated protein content) during 1.5 hours, centrifuged, washed and re-dispersed in water to be analyzed by DLS and z-potential. This assay allow to characterize the species could be formed in following internalization experiments which carried out in the serum media as emulsion of real environment.

Z-potential and size were analysed after the protein enriched serum exposition. Results presented in Table 2 shows how the presence of proteins in media clearly modifies the physico-chemical properties of the surface in almost same magnitude due protein corona formation in all cases.

In general, protein corona makes the nanosystems negatively charged and bulkier than its non-serum treated counterparts.

Table 2. Characterization of MSN-F-MAmBG-n in serum media.

	MSN-F-NH <sub>2</sub>	MSN-F-MAmBG-3	MSN-F-MAmBG-4	MSN-F-MAmBG-5	MSN-F-MAmBG-6
Z-Pot (mV)	-23.4	-22.1	-22.5	-20.8	-21.9
	+40	+29.0	+35.6	+24.2	+35.3
Size (nm)	342	385	400	342	310
	190	190	231	237	226

The data afforded equals the properties of all nanosystems, then, the possible differences of internalization to each other in neuroblastoma cells can be only explained by ligand-receptor interaction, MAmBG-NET in this case.

In order to study the efficacy of the novel targeting agents to enhance the internalization capacity of the nanocarriers, human NB cells were incubated in the presence of each nanomaterial conjugated with the corresponding targeting agent at a fixed

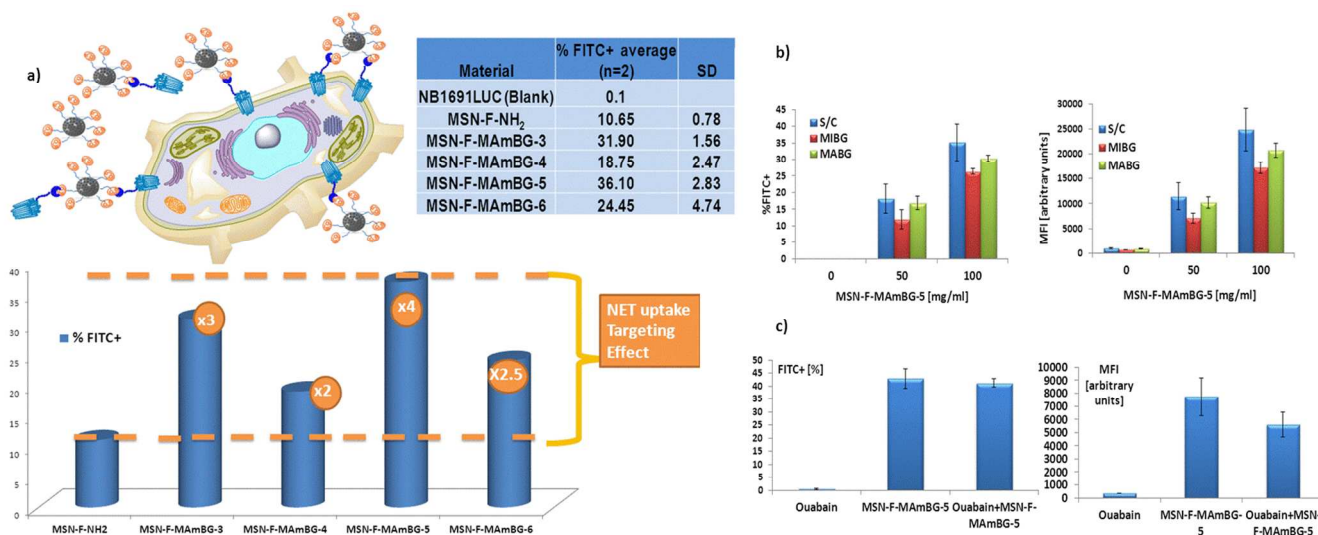


Figure 4. a) Comparative internalization studies in NB cells between all nanosystems synthesized. b) Competitive assays for MSN-F-MAmBG-5 in NB cells with MIBG and MABG. c) Inhibition assays with ouabain for MSN-F-MAmBG-5 (100 µg/ml) in NB cells.

concentration of 100 µg/mL during 2 hours in multiproteic serum culture. After this time, the amounts of cells which had uptaken nanoparticles were determined by flow cytometry measuring the fluorescence at 488 nm as FITC+% representing the percentage of cells with fluorescence. MSN-F-NH<sub>2</sub> was chosen as the negative targeted control, not only by the fact of not being functionalized with targeting agent but also because is strongly positively charged (+40 mV) without serum treatment. The positively charged nanoparticles have shown the greatest efficiency in cell-membrane penetration and cellular internalization.<sup>50</sup> Thus, the use of the MSN-F-NH<sub>2</sub> as negative control; give a realistic idea of internalization capability of the targeted systems competing with a nanosystem with high internalization abilities.

Results showed a notable internalization improvement in all targeted materials comparing with the non-targeted control MSN-F-NH<sub>2</sub>. Short linked derivatives, MSN-F-MAmBG-3 and MSN-F-MAmBG-4 reflected differential behaviour regarding the internalization within NB cells.

The succinic derivate MSN-F-MAmBG-3 internalization is notably higher than its longer linked colleague suberic acid derivate MSN-F-MAmBG-4. This behaviour is fully expected because the difference to each other in terms of percentage of targeting unit grafted in the surface (MSN-F-MAmBG-3, 10.5% w/w versus MSN-F-MAmBG-4, 3% w/w).

Similar effect has been found for long linker derivatives, where the 2 KDa PEGylated derivate MSN-F-MAmBG-5 internalizes four times more than blank MSN-F-NH<sub>2</sub> and possess 0.64 % w/w of targeting groups in contrast with 0.14 % w/w for 10 KDa PEG derivate MSN-F-MAmBG-5 which internalizes almost two times more than the non-targeted material MSN-F-NH<sub>2</sub>.

Thus, comparing between derivatives with proximally properties, the amount of effective targeting is a key parameter. This fact, clearly demonstrates the effect and the influence of targeting

MAmBG moiety grafted in the nanoparticles surface for NB cells internalization proposes. In contrast, the comparison of the better derivatives of both groups (succinic linked MSN-F-MAmBG-3 from short linked group and 2 KDa PEG derivate MSN-F-MAmBG-5 from long linked analogues), reveals obvious alternative effects besides the targeting load effect. MSN-F-MAmBG-3 nanoparticles have showed less potential internalization comparing with 2 KDa PEGylated system MSN-F-MAmBG-5. However the MSN-F-MAmBG-3 is grafted with more than twelve times of targeting agent. This behaviour could be connected with its more external configuration and disposition of the targeting moiety for interaction with NET pocket thanks to PEG linker, making the cellular uptake process more effective, even in presence of proteins in media. This fact improves the selective internalization for NB cells. The external disposition effect presented by 2 KDa PEGylated material, is hidden for 10KDa PEGylated material MSN-F-MAmBG-5. The increase in the length chain involves a dramatic fall of internalization caused by the possible shielding of the targeting moiety from the 10 KDa PEG combined with the low load of recognition moiety in this material surface.

With the aim of confirming the ability of MAmBG derivatives as targeting agents for nanosystems through ligand-receptor interaction, and, considering that, MIBG and norepinephrine are active in the specific uptake-1 mechanism which takes place through the active energy-consuming process by NET. Inhibition and competitive *in vitro* experiments for abolishing the active mechanism of the NET internalization were carried out for the derivate MSN-F-MAmBG-5.

Uptake-1 can be inhibited by saturation of receptor and also through active mechanism blocker. Internalization for the MSN was measured with the presence of the commercially available MIBG (500 µM) and the derivate MABG (500 µM) in parallel assays. These analogues can saturate the cell receptors hampering the nanoparticle uptake directed by NET-grafted

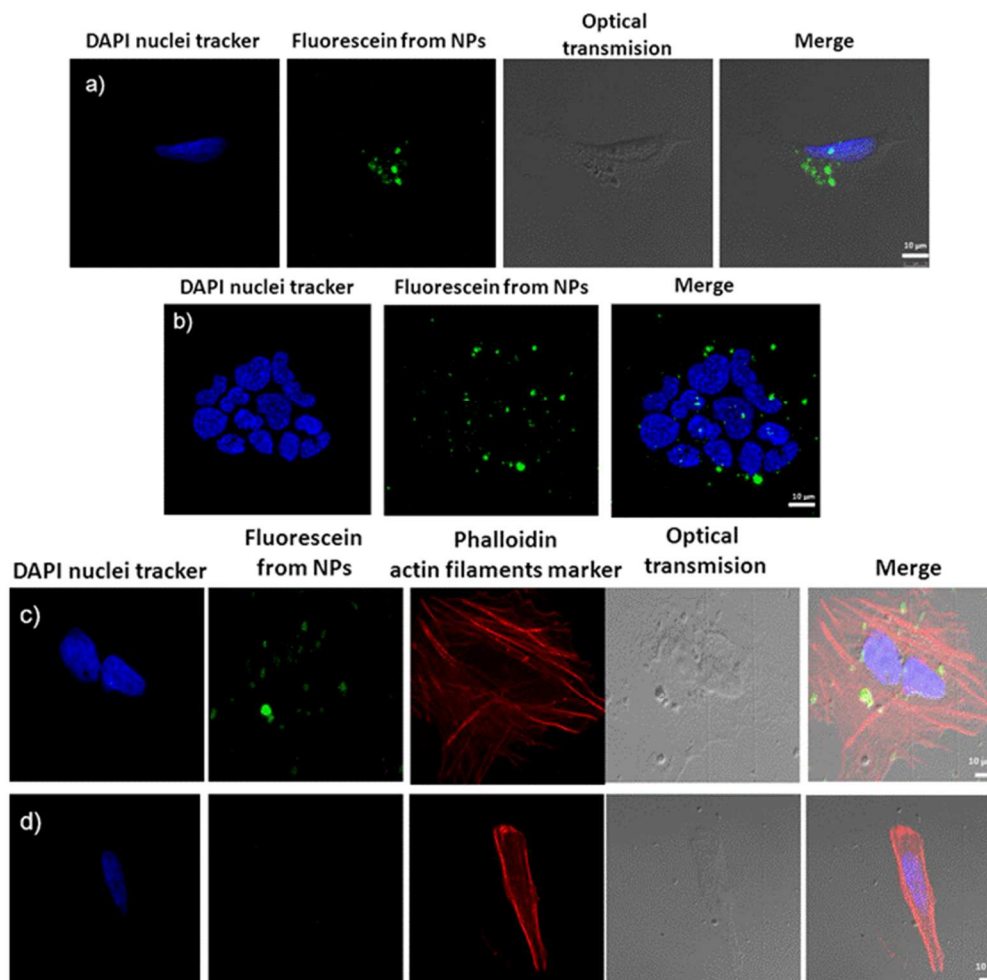


Figure 5. Confocal microscopy pictures. a) and b) Neuroblastoma cells 2h hours of incubation with 100µg/mL of MSN-F-MAmBG-5, blue DAPI for nuclei tracker, washed with glycine/NaCl buffer for eliminating non-internalized nanoparticles in the membrane cell surface. c) Neuroblastoma cells 2h hours of incubation with 100µg/mL of MSN-F-MAmBG-5, blue DAPI for nuclei tracker, phalloidin as actin filaments marker and trypan blue for quenching non-internalized nanoparticles. d) Neuroblastoma cells 2h hours of incubation with 100µg/mL of MSN-F-NH<sub>2</sub>, blue DAPI for nuclei tracker, phalloidin as actin filaments marker and trypan blue for quenching non-internalized nanoparticles.

MAmBG interactions. Internalization in NB cells data were confronted with afforded without any competitive NET receptor in the media. FITC+% measurements reflected a poor decrease of cells with internalized nanoparticles. However, the mean fluorescence indexes (MFI) data, representing intensity of fluorescence per cell, showed an interesting average of 34 % and 14 % of nanoparticles internalization decrease in the NB cells within MIBG and MABG presence respectively in MSN-F-MAmBG-5 concentrations of 50 µg/mL and 100 µg/mL. Thus, the nanocarrier internalization is clearly trending down in excess of MIBG and MABG through saturation of NET.

Furthermore, additional inhibition assays have been carried out abolishing the Na-K-ATPase dependent internalization process of MIBG through NET uptake-1. For this aim, ouabain (1 mM)<sup>22,51</sup> was added to NB cells culture as blocker of energy dependent mechanism before nanoparticles treatment. Internalization of targeted nanovehicles was reduced in 28 %

compared to the internalization results without any blocker in media culture measured as mean fluorescence indexes. All these results suggest that the presence of MAmBG targeting agents in the nanosystems has an important influence in the selective internalization process through NET mediated up-taking. This selective NET-MAmBG interaction is part of the total internalization mechanism of the whole system in NB cells.

In order to confirm the internalization of MAmBG-nanoparticle systems in NB cells, confocal microscopy was applied. The internalization assay was carried out with the derivate MSN-F-MAmBG-5, which exposed the best internalization properties (Figure 5) The accumulation of fluorescent nanoparticles MSN-F-MAmBG-5 (Figure 5 a) b) and c)) in the NB cell cytosol is clearly evident in contrast with the negative control MSN-NH<sub>2</sub> (Figure 5 d)), confirming the higher selectivity and avidity of

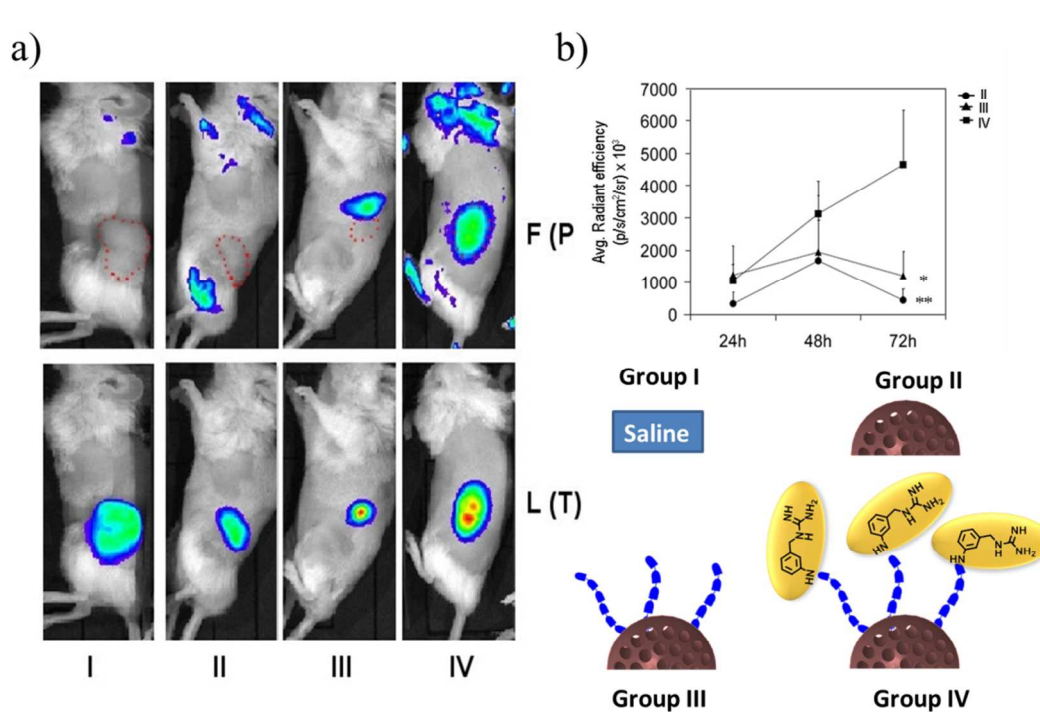


Figure 6. *In vivo* homing of nanoparticles to neuroblastoma. **a)**, *Upper panels*: images show fluorescence signal (F) of nanoparticles (P) 72h after i.v. injection. *Lower panels*: photographs show luminescent emission (L) of tumors (T) derived from s.c. injected NB-Luc. I: saline; II: MSN-Cy7-NH<sub>2</sub>; III: MSN-Cy7-PEG; IV: MSN-Cy7-MAmBG-5. Note co-localization of both fluorescent (nanoparticles) and luminescent (tumor) specifically in MSN-Cy7-MAmBG-5 (IV). Unspecific auto-fluorescence signal can be observed in all groups. **b)**, Graphic shows mean + SD of fluorescence signal in each group 24, 48 and 72h after injection of nanoparticles. II, III and IV as in **A**. Fluorescent signal in saline-injected mice was set as background in all cases. \**p*<0.5 and \*\**p*<0.1 vs. group IV.

the targeted system. The capacity to deliver cytotoxic drugs to NB cells was evaluated as a proof of concept using the best material (MSN-F-MAmBG-5) and doxorubicin hydrochloride as drug model. Increased concentration of drug loaded nanoparticles were administered to NB and mesenchymal cells, selected as negative control due to their lack of NET receptor and their natural presence within the tumoral mass. The results show that more than 20% NB cells died at nanoparticle concentration of 50 µg/mL in only 2 hours whereas mesenchymal cells were barely affected (See SI, Figure S-45). Finally, *in vivo* experiments employing neuroblastoma murine models have been carried out in order to test the real effectiveness of the targeted nanocarrier which presented the best performance in the previous test. In order to monitor the tumor accumulation by IVIS imaging, the nanocarrier was labelled with Cy7 instead of fluorescein because this fluorescent probe is excited in the near infrared region whereas the biological tissues are transparent to this wavelength. This system corresponds to group IV (MSN-Cy7-MAmBG-5). A saline solution (Group I), naked nanoparticles (Group II, MSN-Cy7-NH<sub>2</sub>) and PEGylated nanoparticles without targeting agents (Group III, MSN-Cy7-PEG) were used as controls. A xenograft murine model which presents stably expressing luciferase neuroblastoma tumors is used in order to allow an

easy visualization of the tumoral mass by luminescence measurements.

The results clearly show that the nanoparticles functionalized with the complete targeting system (group IV) present a significant accumulation within the tumoral mass at 48 and 72 hours after the administration, which is clearly visible by the strong fluorescent signal located in the tumoral region. In contrast, the naked and PEGylated particles (groups II and III, respectively) barely exhibited fluorescence in this zone (Figure 6a). It is important to remark that the nanoparticles functionalized with the MABG analogue remain in the tumoral tissue after 72 hours whereas the naked and PEGylated ones are rapidly cleared from the zone (Figure 6b). These findings confirm the efficacy of this targeting agent due to improve not only the selectivity of the nanocarriers but also enhance their retention within the diseased tissue.

## Experimental

### Materials and Methods

Following compounds were purchased from Sigma-Aldrich Inc.: N,N'-methanediyldenebis(propan-2-amine) (DIC), N-hydroxysuccinimide (NHS), N,N-bis(tert-butylloxycarbonyl) guanidine, (3-aminophenyl)methanol, Triphenylphosphine (TPP), Diisopropyl azodicarboxylate (DIAD), Suberic acid

bis(N-hydroxysuccinimide ester (DSS), O,O'-Bis[2-(N-Succinimidyl-succinylamino)ethyl]polyethylene glycol 2KDa and 10KDa, doxorubicin hydrochloride (European Pharmacopoeia), m-Iodobenzylguanidine hemisulfate salt, aminopropyltriethoxysilane (APTES), ammonium nitrate, cetyltrimethylammonium bromide (CTAB), tetraethyl orthosilicate (TEOS). All other chemicals (absolute ethanol, acetone, ethyl acetate heptane, dry solvents etc.) were of the best quality commercially available and they have been employed as received.

#### Characterization techniques.

Powder X-ray diffraction (XRD) experiments were performed with a Philips X'Pert diffractometer equipped with Cu K $\alpha$  radiation (wavelength 1.5406 Å). XRD patterns were collected in the 2 $\theta$  range between 0.6° and 8° with a step size of 0.02° and counting time of 5 s per step. Fourier transform infrared spectroscopy (FTIR) in a Thermo Nicolet nexus equipped with a Goldengate attenuated total reflectance device. The textural properties of the materials were determined by nitrogen sorption porosimetry by using a Micromeritics ASAP 2010. To perform the N<sub>2</sub> measurements, the samples were previously degassed under vacuum for 24 h at room temperature. Thermogravimetry analysis (TGA) were performed in a Perkin Elmer Pyris Diamond TG/DTA analyzer, with 5 °C/min heating ramps, from room temperature to 600 °C. The hydrodynamic size of mesoporous nanoparticles was measured by means of a Zetasizer Nano ZS (Malvern Instruments) equipped with a 633 nm "red" laser. Mass spectra were acquired with a Voyager DE-STR Biospectrometry MALDI-TOF mass spectrometer. Scanning electron microscopy (SEM) analyses were made on a JEOL 6400-LINK AN10000 microscope (Electron Microscopy Centre, UCM). The samples underwent Au metallization previous to observation. Liquid NMR experiments were made in a Bruker AV 250MHz. Solid phase NMR MAS experiments were carried out in a Avance 400MHz. GPC analysis were made in a Waters 2695 with Refractive Index Detector Waters 2414.

#### Calculation procedures.

The surface area was determined using the Brunauer-Emmett-Teller (BET) method and the pore volume,  $V_{\text{pore}}$  (cm<sup>3</sup>·g<sup>-1</sup>), was estimated from the amount of N<sub>2</sub> adsorbed at a relative pressure around 0.99. The pore size distribution between 0.5 and 40 nm was calculated from the desorption branch of the isotherm by means of the Barrett-Joyner-Halenda (BJH) method. The mesopore size,  $\phi_{\text{pore}}$  (nm), was determined from the maximum of the pore size distribution curve.

#### Synthesis of starting amino functionalized nanoparticles MSN-F-NH<sub>2</sub>

FITC (1mg) and APTES (2,2  $\mu$ L) were solved in the minimum volume of EtOH, the mixture was stirred at room temperature for 2 hours under inert atmosphere. The resulting mixture (Solution1) was added under a mixture of TEOS (4.5 mL) and APTES (0.5 mL) also in inert conditions. The resulting mixture

(Solution 2) was added dropwise with gentle stirring under a solution formed by 1g of CTAB, 480 mL of water and 3.5 mL of NaOH 2M at 80 °C. The final reaction mixture was stirred at 80°C during 2 hours. Yellow solid was filtered and washed with water and EtOH.

For template removing, solid was suspended in a solution of NH<sub>4</sub>NO<sub>3</sub> (10 mg/mL) of EtOH/H<sub>2</sub>O in reflux during 48h.

The solid was filtered, washed EtOH and dried in reduce pressure oven at 40°C during 24h. 1.2 g of product was afforded. The solid was functionalized with 6.22x10<sup>-4</sup> mol/gr of amine groups.<sup>52</sup>

#### Synthesis of functionalized nanoparticles MSN-F-MAmBG-n

Compounds (3), (4), (5) and (6) were previously synthesized following Scheme 1. and fully characterized. (See S.I. Section A.1)

For the synthesis of MSN-F-MAmBG-n 100 mg of solid starting material MSN-F-NH<sub>2</sub> (6.22x10<sup>-4</sup>mol/gr primary amines ready to react) were dried under reduce pressure at 80°C placed in a Schlenk during 3 hours. The solid was lead to room temperature and suspended in 20 mL of dried THF, still under inert atmosphere, the dispersion was sonicated during 10 minutes. A solution of 35mg (3), 38 mg (4) (Ratio NH<sub>2</sub>(solid)/acid activated derivate 1:1), 25 mg (5) (Ratio NH<sub>2</sub>(solid)/acid activated derivate 1: 0.20), 64 mg (6) (Ratio NH<sub>2</sub>(solid)/acid activated derivate 1: 0.10) respectively in THF (3 mL) was added dropwise with gentle stirring. The ratios of functionalization process were chosen in order to abolish saturation of the nanoparticles surface in each case. When the addition was finalized the resulted dispersion was warmed to 40 °C overnight.

The resulted yellow solid was washed with THF (3x15mL) and EtOH (3x15) and characterized.

#### General proceed for nanomaterial guanidine deprotection

MSN-F-MAmBG-3-BOC, MSN-F-MAmBG-4-BOC, MSN-F-MAmBG-5-BOC, MSN-F-MAmBG-6-BOC (100 mg in each case) were dried under reduce pressure at 80°C placed in a Schlenk during 3 hours. The solids were lead at room temperature and 10 mL of deprotection cocktail (TFA/DCM 1:1) was added dropwise under inert atmosphere. The mixture was sonicated during 10 minutes and raised to 65°C with gentle stirring 72 hours.

Solid were filtered and washed with DCM, brine and EtOH. Finally, the new materials were dried under vacuum at 40 °C and characterized.

#### Internalization assay

Neuroblastoma cell line NB1691-luc was seeded in 24-well plates at 5000 cells/cm<sup>2</sup>. Cells were exposed to 100  $\mu$ g/ml of MSN-F-NH<sub>2</sub>, MSN-F-MAmBG-3, MSN-F-MAmBG-4, MSN-F-MAmBG-5 or MSN-F-MAmBG-6 for 2 hours at 37°C, 5% CO<sub>2</sub> and 95% humidity. Cells were then washed and harvested. The number of FITC+ cells was evaluated by flow cytometry using the FACSCanto II flow cytometer and the FACSDiva software v6.1.2 (BD Biosciences, San Jose, Ca.). Percentages

of FITC+ populations are shown as the mean of two independent replicates.

### Competition and Inhibition assays

Following the same set up as for the internalization assay 50 µg/ml and 100 µg/ml MSN-F-MAmBG-5 uptake was challenged in the presence of 500 µM MIBG or derivative MABG. Cells were pre-incubated during 15 min with either competitor. After a medium changed containing both MSN-F-AmBG-5 and MIBG or MABG the incubation proceeded for 2 more hours. The inhibition assay with 1mM ouabain was performed as published elsewhere.<sup>22</sup> In both cases, the number of FITC+ cells was evaluated by flow cytometry as in the previous experiment. Mean fluorescence indexes and percentage of FITC+ populations are shown as the mean of two independent replicates.

### Confocal Imaging

For confocal analysis cells were seeded on glass chamber slides (LabTek II, Nunc, Rochester, NY) and incubated with 100 µg/ml MSN-F-AmBG-5 or MSN-F-NH<sub>2</sub> for 2 hours. Internalization was stopped by washing cells with ice-cold PBS followed by two acid washes with 250mM NaCl, 100mM glycine pH 2.5 to remove any adsorbed particles. Cells were then fixed in 4% PFA, stained with Texas Red-X phalloidin (Molecular Probes, Eugene, OR) and mounted in DAPI-containing Fluoroshield (Sigma, St. Louis, MO). Images were capture via a 63×/1.4 oil-immersion objective on the Leica SP5 confocal microscope and the Leica LAS AF software.

### In vivo homing/biodistribution assays.

Human neuroblastoma NB-1691 cells (kindly provided by Dr. Antonio Pérez, Hospital La Paz, Madrid) were transduced with pHRSIN-CS-Luc-IRES-emGFP-WdlNotI lentiviral vector (kindly provided by Dr. Antonio Rodríguez, Universidad Autónoma de Madrid) in order to generate a stably expressing luciferase neuroblastoma cell line (NB-Luc). 2.5x10<sup>6</sup> NB-Luc cells were subcutaneously injected into the left flank of NOD.Cg-Prkd<sup>escid</sup> Il2rg<sup>tm1Wjl</sup>/SzJ (NSG; Jackson) immunodeficient mice. Three weeks later, 200µl of saline (group I) or 1mg of either Cy7-labeled bare nanoparticles (group II), PEG-covered nanoparticles (group III) or MIBG-PEG-covered nanoparticles (group IV), were inoculated i.v. into these mice. *In vivo* biodistribution of Cy7-labeled nanoparticles was monitored through fluorescent image acquisition in an IVIS Lumina XRMS (Perkin Elmer) at 24, 48 and 72h after nanoparticles injection. The presence and localization of NB-Luc-derived tumors was confirmed through the detection of luminescent signal after i.p. injection of 1.25mg/mice D-Luciferin (Perkin Elmer). Image analysis was performed with Living Image® 4.4 software (Perkin Elmer). Animal studies were in accordance with the guidelines of the EU on animal care (2010/63/EU) and approved by the institutional ethics committee (Comité de Ética de la

Investigación y Bienestar Animal ISCIII; procedure CBA PA 25\_2011-v2).

### Conclusions

In conclusion, different novel targeting agents based on MIBG structure have been synthesized and grafted on the surface of mesoporous silica nanoparticles, employed as carrier model. This type of structure has been chosen due to the well-known affinity of MIBG for the norepinephrine transporter which is highly expressed by neuroblastoma cells. The efficacy of each targeting agent to induce an enhanced nanocarrier cellular uptake have been tested using neuroblastoma cell line NB1691-luc, showing in the best case an increase of up to four times. This system was able to work in a serum multi-proteic media, keeping the targeting properties of the grafted agent coexisting with protein corona effect. Furthermore, drug loaded targeted nanoparticles showed high exclusive cytotoxic effect in NB cells. Finally, the *in vivo* efficacy of these carriers was tested using murine neuroblastoma models. The results indicate that the surface functionalization with these targeting agents provokes a significative higher tumoral tissue accumulation and retention in comparison with the non-decorated particles. This type of selective targeting agents could be easily applied to different nanoparticle platforms paving the way for the application of novel nanomedicines for the treatment of neuroblastoma.

### Acknowledgements

This work was supported by the Ministerio de Economía y Competitividad, through project MAT2012-35556, CSO2010-11384-E (Ageing Network of Excellence) and CIBER-BBN and ECO Foundation through project Smart4NB. We also thank the X-ray Diffraction C.A.I. and the National Electron Microscopy Center, UCM.

### Notes and references

<sup>a</sup> Dpto. Química Inorgánica y Bioinorgánica. Instituto de Investigación Sanitaria Hospital, 12 de Octubre i+12.UCM. Centro de Investigación Biomédica en Red de Bioingeniería, Biomateriales y Nanomedicina (CIBER-BBN). Madrid, Spain.

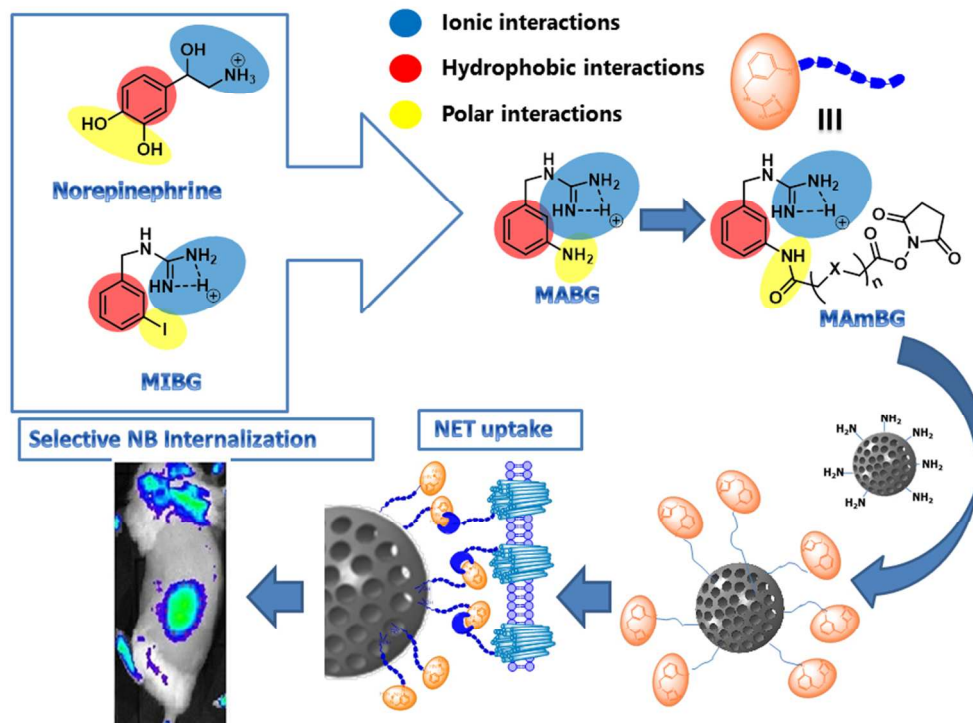
<sup>b</sup> Dpto. de Hematología y Oncología Pediátricas, Hospital Infantil Universitario Niño Jesús, Madrid, Spain.

<sup>c</sup> Servicio de Inmunología. Hospital Universitario de La Princesa. Diego de León, 62. 28006 Madrid, Spain.

Electronic Supplementary Information (ESI) available: Experimental proceeds for synthesis of the organic precursors. Additional spectra information; FTIR, NMR, XRD, BET, size distributions. UV determination of targeting units for pegylated derivatives. See DOI: 10.1039/b000000x/

- 1 S. Marchesan and M. Prato, *Acs Med. Chem. Lett.*, 2013, **4**, 147–149.
- 2 N. Ž. Knežević and J.-O. Durand, *Chempluschem*, 2015, **80**, 26–36.
- 3 I. Brigger, C. Dubernet and P. Couvreur, *Adv. Drug Deliv. Rev.*, 2012, **64**, 24–36.

- 4 I.-J. Fang, I. I. Slowing, K. C.-W. Wu, V. S.-Y. Lin and B. G. Trewyn, *Chemistry*, 2012, **18**, 7787–92.
- 5 J. Sun, D.-H. Kim, Y. Guo, Z. Teng, Y. Li, L. Zheng, Z. Zhang, A. C. Larson and G. Lu, *J. Mater. Chem. B*, 2015, **3**, 1049–1058.
- 6 G.-F. Luo, W.-H. Chen, Y. Liu, J. Zhang, S.-X. Cheng, R.-X. Zhuo and X.-Z. Zhang, *J. Mater. Chem. B*, 2013, **1**, 5723–5732.
- 7 Z. Tang, D. Li, H. Sun, X. Guo, Y. Chen and S. Zhou, *Biomaterials*, 2014, **35**, 8015–27.
- 8 C. Chen, J. Ke, X. E. Zhou, W. Yi, J. S. Brunzelle, J. Li, E.-L. Yong, H. E. Xu and K. Melcher, *Nature*, 2013, **500**, 486–9.
- 9 J. Wang, P. P. Gao, X. X. Yang, T. T. Wang, J. Wang and C. Z. Huang, *J. Mater. Chem. B*, 2014, **2**, 4379.
- 10 Q. Zhang, X. Wang, P.-Z. Li, K. T. Nguyen, X.-J. Wang, Z. Luo, H. Zhang, N. S. Tan and Y. Zhao, *Adv. Funct. Mater.*, 2014, **24**, 2450–2461.
- 11 C. H. Wu, Y. P. Chen, S. H. Wu, Y. Hung, C. Y. Mou and R. P. Cheng, *ACS Appl. Mater. Interfaces*, 2013, **5**, 12244–12248.
- 12 J. Li, F. Liu, Q. Shao, Y. Min, M. Costa, E. K. L. Yeow and B. Xing, *Adv. Healthc. Mater.*, 2014, **3**, 1230–1239.
- 13 Y. P. Chen, C. T. Chen, Y. Hung, C. M. Chou, T. P. Liu, M. R. Liang, C. T. Chen and C. Y. Mou, *J. Am. Chem. Soc.*, 2013, **135**, 1516–1523.
- 14 F. Chen, H. Hong, Y. Zhang, H. F. Valdovinos, S. Shi, G. S. Kwon, C. P. Theuer, T. E. Barnhart and W. Cai, *ACS Nano*, 2013, **7**, 9027–9039.
- 15 F. Chen, T. R. Nayak, S. Goel, H. F. Valdovinos, H. Hong, C. P. Theuer, T. E. Barnhart and W. Cai, *Mol. Pharm.*, 2014, **105**.
- 16 S. Veerananarayanan, A. C. Poulouse, M. S. Mohamed, S. H. Varghese, Y. Nagaoka, Y. Yoshida, T. Maekawa and D. S. Kumar, *Small*, 2012, **8**, 3476–3489.
- 17 F. Danhier, O. Feron and V. Preat, *J. Control. Release*, 2010, **148**, 135–146.
- 18 S. Sengupta and A. Kulkarni, *ACS Nano*, 2013, **7**, 2878–2882.
- 19 D. Hanahan and R. a Weinberg, *Cell*, 2011, **144**, 646–74.
- 20 J. M. Maris, *N. Engl. J. Med.*, 2010, **362**, 2202–2211.
- 21 E. Ruoslahti, S. N. Bhatia and M. J. Sailor, *J. Cell Biol.*, 2010, **188**, 759–768.
- 22 R. J. Mairs, M. N. Gaze and A. Barrett, 1991, **295**, 293–295.
- 23 K. K. Matthay, R. E. George and A. L. Yu, *Clin. Cancer Res.*, 2012, **18**, 2740–53.
- 24 J. P. Howard, J. M. Maris, L. S. Kersun, J. P. Huberty, S.-C. Cheng, R. a Hawkins and K. K. Matthay, *Pediatr. Blood Cancer*, 2005, **44**, 232–9.
- 25 S. Ekelund, P. Nygren and R. Larsson, *Biochem. Pharmacol.*, 2001, **61**, 1183–93.
- 26 a Kuin, M. Aalders, M. Lamfers, D. J. van Zuidam, M. Essers, J. H. Beijnen and L. a Smets, *Br. J. Cancer*, 1999, **79**, 793–801.
- 27 A. Schlessinger, E. Geier, H. Fan, J. J. Irwin, B. K. Shoichet, K. M. Giacomini and A. Sali, *Proc. Natl. Acad. Sci. U. S. A.*, 2011, **108**, 15810–5.
- 28 G. Vaidyanathan, S. Shankar and M. R. Zalutsky, 2001, 786–797.
- 29 G. Vaidyanathan, S. Shankar, D. J. Affleck, P. C. Welsh, S. K. Slade and M. R. Zalutsky, 2001, 798–806.
- 30 G. Vaidyanathan, P. C. Welsh, K. C. Vitorello, S. Snyder, H. S. Friedman and M. R. Zalutsky, *Eur. J. Nucl. Med. Mol. Imaging*, 2004, **31**, 1362–70.
- 31 D. Hadrich, F. Berthold, E. Steckhan and H. Bönisch, *J. Med. Chem.*, 1999, **42**, 3101–8.
- 32 G. Vaidyanathan, S. Shankar, D. J. Affleck, K. Alston, J. Norman, P. Welsh, H. LeGrand and M. R. Zalutsky, *Bioorg. Med. Chem.*, 2004, **12**, 1649–56.
- 33 W. Wang, J. Shohet, M. Mawad and S. Ke, *US Pat. App. 13/638,060*, 2011.
- 34 M. Vallet-Regí, A. Rámila, R. P. del Real and J. Pérez-Pariente, *Chem. Mater.*, 2001, **13**, 308–311.
- 35 A. Baeza, M. Colilla and M. Vallet-Regí, *Expert Opin. Drug Deliv.*, 2014, 1–19.
- 36 V. Mamaeva, C. Sahlgren and M. Lindén, *Adv. Drug Deliv. Rev.*, 2013, **65**, 689–702.
- 37 M. Vallet-Regí and E. Ruiz-Hernández, *Adv. Mater.*, 2011, **23**, 5177–218.
- 38 Z. Li, J. C. Barnes, A. Bosoy, J. F. Stoddart and J. I. Zink, *Chem. Soc. Rev.*, 2012, **41**, 2590–605.
- 39 C. Sanchez, C. Boissiere, S. Cassaignon, C. Chaneac, O. Durupthy, M. Faustini, D. Grosso, L. Nicole, D. Portehault, F. Ribot, L. Rozes and C. Sasseoye, 2014.
- 40 A. Baeza, E. Guisasola, A. Torres-Pardo, J. M. González-Calbet, G. J. Melen, M. Ramirez and M. Vallet-Regí, *Adv. Funct. Mater.*, 2014, **24**, 4625–4633.
- 41 W. E. R. N. E. R. Stober, 1968, **69**, 62–69.
- 42 A. Van Blaaderen and A. Vrij, 1992, **81**, 2921–2931.
- 43 D. S. Dodd and A. P. Kozikowski, 1994, **35**, 977–980.
- 44 H. Meng, M. Xue, T. Xia, Z. Ji, D. Y. Tarn, J. I. Zink and A. E. Nel, *ACS Nano*, 2011, **5**, 4131–44.
- 45 Q. He, J. Zhang, J. Shi, Z. Zhu, L. Zhang, W. Bu, L. Guo and Y. Chen, *Biomaterials*, 2010, **31**, 1085–1092.
- 46 A. Salvati, A. S. Pitek, M. P. Monopoli, K. Prapainop, F. B. Bombelli, D. R. Hristov, P. M. Kelly, C. Åberg, E. Mahon and K. a Dawson, *Nat. Nanotechnol.*, 2013, **8**, 137–43.
- 47 R. Gaspar, *Nat. Nanotechnol.*, 2013, **8**, 79–80.
- 48 P. Verderio, S. Avvakumova, G. Alessio, M. Bellini, M. Colombo, E. Galbiati, S. Mazzucchelli, J. P. Avila, B. Santini and D. Prospero, *Adv. Healthc. Mater.*, 2014, **3**, 957–76.
- 49 J. Townson, Y. Lin and J. Agola, *J. Am. Chem. Soc.*, 2013, **135**, 16030–16033.
- 50 A. Verma and F. Stellacci, *Small*, 2010, **6**, 12–21.
- 51 K. A. Streby, N. Shah, M. A. Ranalli, A. Kunkler and T. P. Cripe, 2015, 5–11.
- 52 Y. Zhang and Y. Chen, *IET Nanobiotechnol.*, 2012, **6**, 76–80.



Novel MIBG analogues as targeting agents for neuroblastoma nanomedicines.  
254x190mm (96 x 96 DPI)